Available online at www.sciencedirect.com
SCIENCE DIRECT
Journal of Photochemistry and Photobiology A: Chemistry 178 (2006) 33–40
Journal of Photochemistry and Photobiology A:Chemistry
www.elsevier.com/locate/jphotochem

Interconnecting dye solar cells in modules—*I–V* characteristics under reverse bias

R. Sastrawan [b,*], J. Renz [a], C. Prahl [a], J. Beier [c], A. Hinsch [a], R. Kern [a]

[a] *Fraunhofer Institute for Solar Energy Systems, Heidenhofstr. 2, D-79110 Freiburg, Germany*
[b] *Freiburg Materials Research Centre, Stefan-Meier Str. 21, 79104 Freiburg, Germany*
[c] *Institut für Angewandte Photovoltaik, Munscheidstrasse 14, D-45886 Gelsenkirchen, Germany*

Received 2 May 2005; received in revised form 16 June 2005; accepted 20 June 2005
Available online 26 July 2005

Abstract

The upscaling of the dye solar cell (DSC) technology involves a series connection of single cells to form modules. Thus an utilisable voltage is reached. In an outdoor situation, one or more cells connected in series might be shaded. The shaded cells then have to transport the current of the module in reverse bias.

Here, a study of the processes and interfaces involved in the electron transport of a DSC under reverse bias is presented. Furthermore, the effect of these processes on the long-term stability of a DSC is evaluated.

The *I–V* characteristic of a DSC under reverse bias differs significantly from a typical diode *I–V* characteristic. Compared to other solar cell technologies, in particular crystalline silicon solar cells, the largest sustainable reversed biased voltage (breakdown voltage) of a DSC is extremely low (approximately 500 mV). Therefore, in terms of power output, no bypass diodes are required, when connecting DSC in series.

In order to identify the processes and the interfaces involved in the charge carrier transport in reverse bias, a batch of different electrode set-ups was built that consisted of single components of a standard DSC.

It was shown that charge transport under reverse bias directly occurs via the electrolyte/TCO (transparent conducting oxide) interface, catalysed by the dye molecules. The charge transfer is highly asymmetrical, with a symmetry parameter of approximately 0.35, using a simple Butler-Vollmer model.

Electrical impedance spectroscopy revealed that the TiO_2-layer is not significantly involved in the electron transport under reverse bias.

To study the effect of reverse biasing on the long-term stability of DSC, solar cells were subjected to a constant reverse current in the dark for more than 100 h. The voltage drop over the cell was monitored. It increased only slightly, without reaching critical values, which would damage the cell irreversibly. No degradation in overall efficiency was observed for more than 100 h.

Keywords: Dye sensitized; Reverse; Modules; Series; Shading

1. Introduction

Dye solar cells (DSC) developed by Gratzel and co-workers [1,2] have achieved solar power efficiencies over 10% on small areas [3]. Because of their potential low production costs and the attractive colour design [4], considerable efforts are being increasingly undertaken to enable a commercial upscaling of this new type of solar cell. Good progress was made in the fields of technical performance, manufacturability [5,6], long-term stability [7,8] and large area module design [9–12]. Most concepts for large area DSC modules involve a series interconnection between a large numbers of cells in order to receive an utilisable voltage.

* Corresponding author. Tel.: +49 761 4588 5361; fax: +49 761 4588 9000.
E-mail address: Ronald.Sastrawan@fmf.uni-freiburg.de (R. Sastrawan).

1010-6030/$ – see front matter © 2005 Elsevier B.V. All rights reserved.
doi:10.1016/j.jphotochem.2005.06.017

As in all types of solar cells, the partial shading of a photovoltaic array has to be considered. If one cell in a series connection of solar cells is shaded, the current of the module has to pass this shaded cell in reverse bias.

Two different types of series connections can be found in commercial solar modules. The individual solar cells are connected externally and are then assembled into a solar module. This technique is commonly used for crystalline silicon modules. The second option, as in thin film solar modules, is that all cells of the module are manufactured simultaneously already with an integrated series connection.

In crystalline silicon solar cells, the largest sustainable reverse biased voltage (breakdown voltage) can be greater than 20 V [13]. At breakdown voltage, a reverse current flows due to the avalanche breakdown, the shaded cell becomes an energy load rather than an energy producer. Hot spots, points of localised overheating with temperatures of more than 150 °C, occur and may cause cell cracking and damage to module encapsulation. Therefore, bypass diodes are incorporated across individual cells or groups of cells. The verification of hot-spot resistance is part of test standard IEC 61215 for crystalline silicon modules [14].

Thin-film modules are usually manufactured as integrated circuits with integrated series connections. The individual cells are not accessible, so bypass diodes can only be installed across module terminals. Hence, hot-spot protection is not possible. On the other hand, thin-film modules have a striped pattern, making the extensive shading of a single cell very unlikely under outdoor operation. The product qualification testing for thin-film modules includes the verification of hot-spot resistance in accordance with IEC 61646 [15].

No matter what type of series connection is implemented for DSC modules, the reverse biased *I–V* characteristic of DSC must be understood. Models have been developed to explain and analyse the behaviour of DSC under forward bias, but usually not under reverse bias [16–23]. However, the dominating current route in reverse bias (substrate/electrolyte interface) is also an important loss mechanism under forward bias [24]. In this paper, we investigate the processes involved in the electron transport under reverse bias with special attention to a series connection of DSC.

Furthermore, the long-term stability of a DSC operated in reverse bias is investigated. Studies on DSC have been reported previously, which showed that a reverse biased potential of ∼1500 mV could result in a degradation of the cell's performance, due to damaging of the dye [25]. However, in a realistic module design, the maximum current conducted through the shaded solar cell would be equivalent to its own short-circuit current. When this is the case, the voltage drop is much lower, as will be shown in this paper.

2. Theory

In crystalline silicon solar cells, first at large reverse bias voltages, the so-called breakdown voltage, a sharp rise in the current occurs due to the avalanche breakdown. The value of this largest sustainable reverse biased voltage varies and can be 20 V or greater.

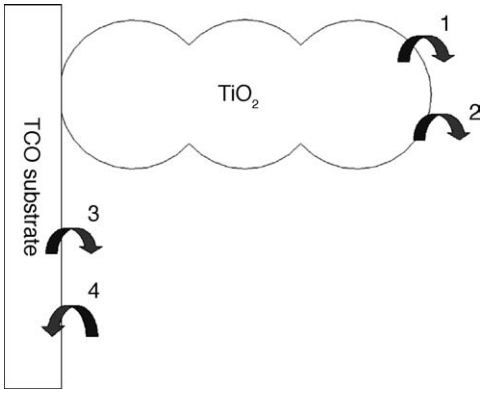

Fig. 1. The four routes of electron transfer 1 and 2 are the recombination of TiO_2 conduction band electrons and surface state electrons with the electrolyte under forward bias, respectively. Route 3 is the reduction of I_3^- at the TCO substrate under forward bias. Route 4 is the oxidation of I^- at the TCO substrate under reverse bias.

In a DSC, current flows in reverse bias, but no actual 'breakdown' occurs. Also, the current will not rise as steeply. Nevertheless, the term breakdown voltage will be used in this paper to describe the reverse biased voltage, which is required to obtain a reverse current in the magnitude of the short-circuit current of the cell, i.e. about 20 mA/cm^2.

Under forward bias, electron recombination mainly occurs from the TiO_2 conduction band or surface states with the electrolyte (Fig. 1, Processes 1 and 2). Electron recombination by reduction of the I_3^- ions at the TCO substrate (transparent conducting oxide) can be neglected under short-circuit conditions, but becomes important at open-circuit conditions (Fig. 1, Process 3). Especially under low light intensities, the back reaction of electrons via the TCO substrate is the dominant route [24].

Under reverse bias, electron transfer mainly occurs via the TCO/electrolyte interface by oxidation of the I^- ions (Fig. 1, Process 4). A compact TiO_2 blocking layer can suppress this route [26,27]. However, in this work for DSC modules an easy electron transfer under reverse bias over the substrate is desired. Therefore, blocking layers have not been applied.

If no blocking layer is present, the TCO behaves essentially as a non-catalytic metal, and in the absence of diffusion limitations, the total current density for the electron-transfer redox reaction

$$I_3^- + 2e^- \Leftrightarrow 3I^- \quad (1)$$

is given by the Butler-Vollmer equation, which can be written in terms of the overvoltage as [28]:

$$j = j_0(e^{\beta(e_0/kT)V} - e^{-(1-\beta)(e_0/kT)V}) \quad (2)$$

The relation between the current density j and the overvoltage V is determined by two parameters: the exchange current density j_0 and the symmetry parameter β.

The exchange current density varies on the type of TCO glass used, as well as on thermal treatment of the glass [24]. Adsorbed impurities on the TCO may act as catalytic sites. In this paper, we will show that in particular, the dye molecules are adsorbed to the TCO substrate and catalyse the electron transfer reaction. In this case, the symmetry parameter greatly differs from 0.5, favouring one direction of the electron exchange.

3. Experimental

3.1. Cell preparation

All electrode set-ups were manufactured on so-called masterplates [7]. One masterplate consists of five individual cells of 5 cm × 0.5 cm on a SnO_2:F-glass substrate (LOF-TEC 8, 3 mm, 8 Ω/square). All layers were applied by screen-printing.

Screen printable TiO_2 paste was prepared by dispersing commercial TiO_2 nanoparticles of sizes between 20 nm and 40 nm in a 90:10 terpineol/ethylcellulose mixture using a pearl mill. A layer thickness of about 10 μm was obtained by screen-printing two subsequent layers.

Platinum paste was obtained by mixing H_2PtCl_6 from Aldrich with terpineol and ethylcellulose.

A screen-printed silver strip (paste from Ferro) on each side of each cell ensured proper current collection within the masterplate.

For the primary sealing a screen printable glass frit paste was applied on both electrodes [7].

After all layers had been deposited, front and counter electrodes were sintered at 450–500 °C for 30 min. The sealing (fusing) of the masterplate was done at 630 °C for 30 min. The electrode spacing was about 30 μm in this case.

N719 dye was purchased from Solaronix S.A. in Switzerland. A 1 mM dye solution in 50:50 acetonitrile/*tert*-butanol was pumped through each cell via holes using a coloration machine purchased from Energy Research Centre Netherlands (ECN) [6].

Finally, each cell was flushed with acetonitrile, dried with nitrogen and filled with electrolyte. The filling holes were closed with a Surlyn 1702 hotmelt foil and a thin glass cover.

The electrolyte composition was 0.6 M hexylmethylimidazolium iodide (HMII); 0.1 M LiI; 0.05 M I_2; 0.5 M *tert*-butyl pyridine (TBP) in acetonitrile.

3.2. Apparatus

I–V characteristics were measured using a Keithley 230. If needed, illumination was supplied by halogen lamps, calibrated with a silicon cell, taking into account the spectral mismatch.

All electrical impedance measurements were carried out in the dark with an impedance measurement unit (IM 6) from Zahner. The amplitude of the modulated voltage was 5 mV.

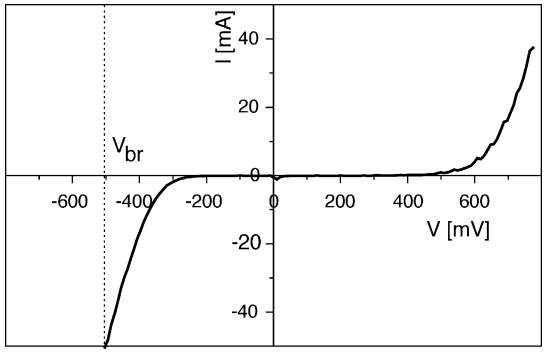

Fig. 2. Measured *I–V* curve of a typical DSC (area = 2.5 cm^2) in the dark. The breakdown voltage (V_{br}) is at −500 mV.

4. Results and discussion

4.1. Reverse biasing a DSC and series connection

Fig. 2 shows a typical *I–V* curve of a DSC (area = 2.5 cm^2) in the dark. The breakdown voltage (V_{br}) of about −500 mV is extremely low compared to crystalline silicon solar cells. This is an advantage when connecting solar cells in series. The power output of a solar module is much less sensitive to partial shading when each solar cell has a low breakdown voltage.

In a series connection the total voltage is determined by the sum of the voltages of each cell for every current. Fig. 3 shows *I–V* curves of five identical DSC connected in series without bypass diodes.

When one cell is completely shaded, the open-circuit voltage is reduced by the open-circuit voltage of this cell (about 700 mV) plus the voltage required to run the shaded cell in reverse bias (about 300 mV). The short-circuit current is only reduced very slightly, because of the low breakdown voltage of the shaded cell. A similar behaviour is obtained as with crystalline silicon cells with installed bypass diodes.

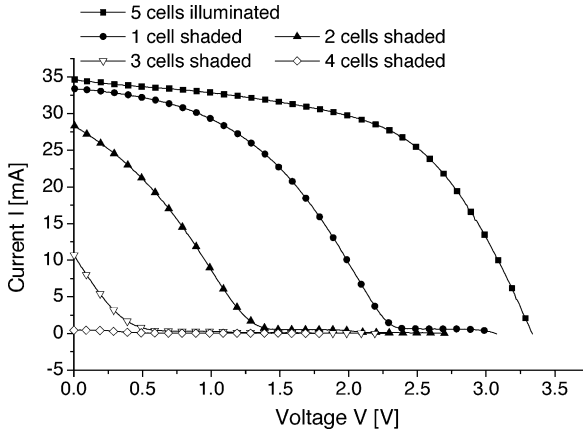

Fig. 3. Measured *I–V* curves under illumination (1000 W/m^2) of an array of five DSC connected in series. The cells are successively shaded completely.

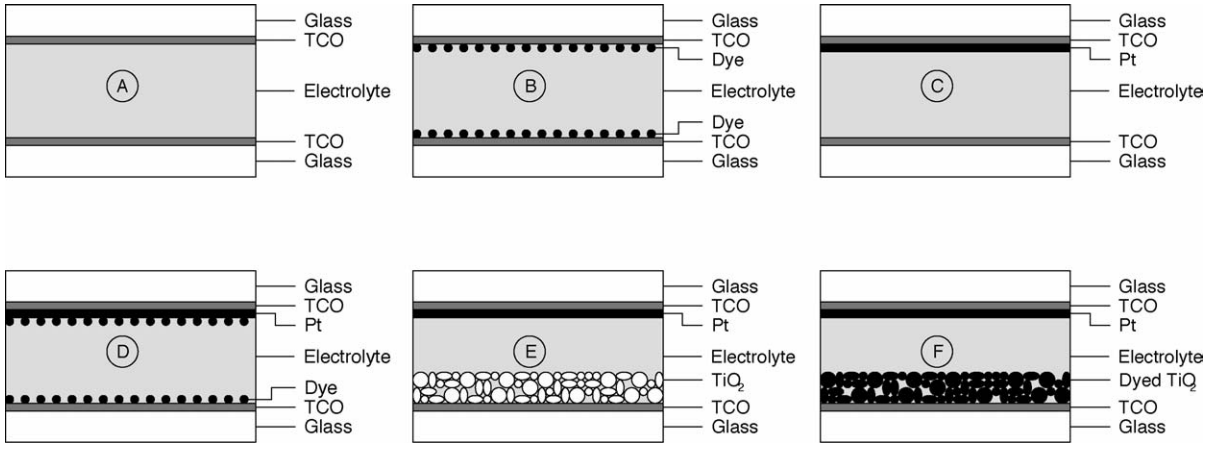

Fig. 4. Special electrode set-ups used for the experimental analysis of the electron transport in DSC under reverse bias. For explanation see text.

4.2. Charge carrier transport in reverse-bias

In order to identify the processes and the interfaces involved in the charge carrier transport under reverse bias, six electrode set-ups that consisted of single components of a standard DSC (Fig. 4) were built. Set-up A consists of two TCO-electrodes and the electrolyte. Set-up B consists of TCO-electrodes that have been flushed with dye before injecting the electrolyte. Set-up C consists of one platinum-coated electrode and one TCO-electrode and electrolyte. Set-up D is the same as C, only flushed with dye before injecting the electrolyte. Set-up E is a standard DSC set-up without dye (TCO/Pt/electrolyte/TiO_2/TCO). Set-up F is a standard DSC flushed with dye.

In the following, a negative platinum electrode is referred to as reverse bias (electron transport from the platinum electrode to the electrolyte), and a positive platinum electrode is referred to as forward bias (electron transport from the electrolyte to the platinum electrode), as illustrated in Fig. 5.

Fig. 6 shows the *I–V* curves of set-ups A–E measured in the dark. As can be seen, set-ups A (TCO/electrolyte/TCO) and B (TCO/electrolyte/TCO flushed with dye) do not conduct any current at applied biases from −1.5 to +1.5 V.

If one electrode is coated with platinum (set-up C), the charge transfer resistance at the platinum electrode is reduced drastically. The resistance of the platinum/electrolyte interface may be neglected when compared to the uncoated TCO/electrolyte interface. The *I–V* characteristic is now determined by the charge transfer reaction at the TCO/electrolyte interface and can be described by the Butler-Vollmer equation at the TCO/electrolyte electrode (Eq. (2)).

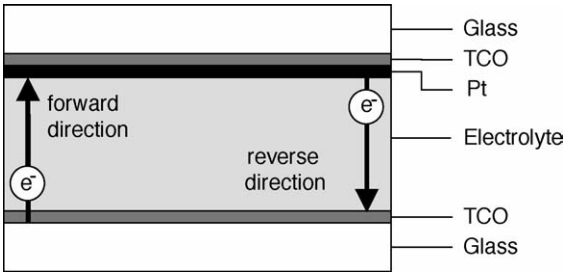

Fig. 5. Definition of forward and reverse direction of electrons in the electrode set-ups. $U > 0$: forward bias, $U < 0$: reverse bias.

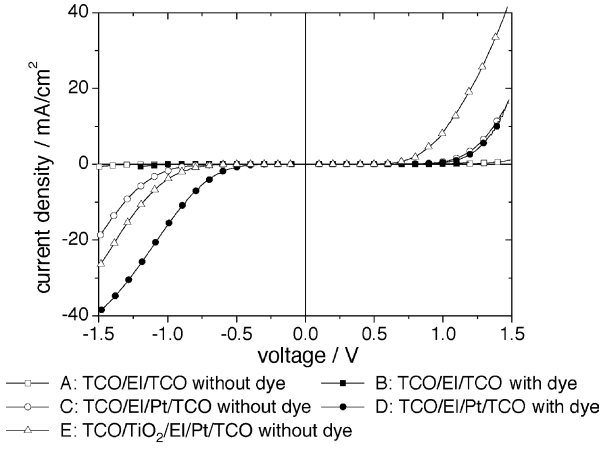

Fig. 6. Measured *I–V* curves of set-ups A–E measured in the dark.

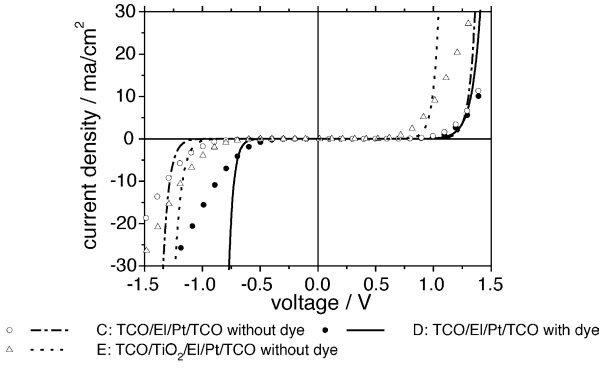

Fig. 7. The *I–V* curves of set-ups C–E were fitted to the Butler-Vollmer equation. The fit parameters were: C: $j_0 = 1.4 \times 10^{-10}$ mA/cm^2; $\beta = 0.50$; D: $j_0 = 1.4 \times 10^{-7}$ mA/cm^2; $\beta = 0.35$; E: $j_0 = 9.5 \times 10^{-9}$ mA/cm^2; $\beta = 0.54$.

In Fig. 7, the Butler-Vollmer equation is fitted to *I–V* curves of set-ups C–E. The fits do not agree very well to the experimental results, because the Butler-Vollmer equation only describes the electron transfer at one TCO/electrolyte interface. The charge transport in the electrolyte and the charge transfer at the platinum electrode are neglected in this approach. However, the fits very well account for the asymmetric behaviour of the measured *I–V* characteristics.

The reaction at the TCO/electrolyte interface of set-up C is symmetric, yielding a symmetry parameter of $\beta = 0.5$.

When the TCO/electrolyte interface is covered with dye molecules (set-up D), the exchange current density over this interface increases over 3 magnitudes and the symmetry parameter is about 0.35. In other words, the dye catalyses the electrons transfer from the electrolyte to the TCO (reverse biasing). The direction from the TCO to the electrolyte (forward biasing) seems unaffected.

Presumably, the dye participates in the electron transfer reaction under reverse bias. It is likely that the dye is being oxidised at voltages of about 0.5 V. This oxidation is reversible as the dye is being reduced by the iodide again.

When the TCO is coated with a nanocrystalline layer of TiO_2 (set-up E), a symmetry parameter of $\beta = 0.54$ is obtained. In this case, the Butler-Vollmer equation is not at all suited to describe *I–V* characteristic. It is only used to determine a symmetry parameter for comparison.

Nevertheless, *I–V* curve of set-up E shows that the electron transfer from the electrolyte to the TCO (reverse biasing) is not significantly affected by the nanoporous TiO_2 layer. However, the electron transfer from the TCO to the electrolyte (forward biasing) is facilitated by the TiO_2. The involved processes of electron transport in the nanocrystalline TiO_2 and the electron recombination from the TiO_2 to the electrolyte are well known from detailed models and studies describing the DSC under forward bias in the dark [18,20,29].

4.3. Interfaces studied by electrical impedance spectroscopy

Electrode set-ups C, D and F were studied using electrical impedance spectroscopy (EIS). All EIS measurements were carried out in the dark with different bias voltages. The amplitude of the modulated voltage was 5 mV.

Fig. 8 shows the impedance of set-up C (TCO/Pt/electrolyte/TCO) compared to set-up D (TCO/Pt/electrolyte/TCO flushed with dye) at a reverse biased voltage of −0.8 V. Without the dye (C), the impedance is determined by the high resistance of the TCO/electrolyte interface. When dye molecules are attached to the TCO electrode (D), the resistance drops by one magnitude under reverse bias. In addition to the peak in the phase at 10 kHz associated with the Pt/electrolyte interface [30], a peak is visible at about 500 Hz, which can be associated with the electron transfer at the TCO/dye/electrolyte interface. The resistance of the TCO/dye/electrolyte interface now has a magnitude, which

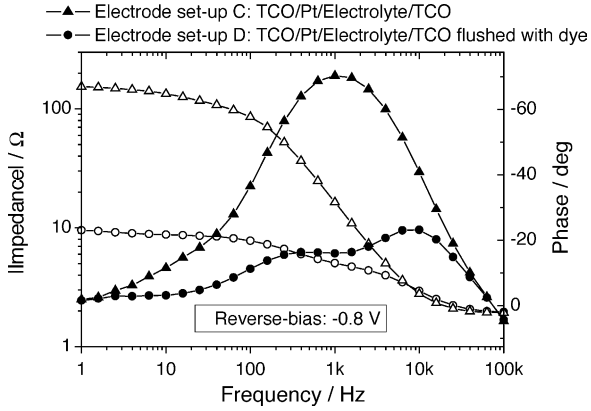

Fig. 8. Measured EIS of set-ups C and D under reverse bias of −0.8 V. Open symbols: |*Z*|; solid symbols: phase (*Z*).

is approximately equivalent to that of the Pt/electrolyte interface.

Fig. 9 again shows the impedance of set-up D (TCO/Pt/electrolyte/TCO flushed with dye), at reverse and forward biased voltages of −0.8 and +0.8 V. Under a forward bias of +0.8 V, the TCO/dye/electrolyte interface acts like set-up C: the dye is not catalysing the electron transfer in this direction. Under reverse bias the dye catalyses the electron transfer. The resistance drops and the two peaks associated with the platinum/electrolyte interface and TCO/dye/electrolyte interface are visible, like in Fig. 8.

Fig. 10 shows the impedance of set-up F (a complete DSC) at reverse and forward biased voltages of +0.8 and −0.8 V. A phase peak at about 10 Hz is associated with electrons recombining from the TiO_2 to the electrolyte, and a phase peak at about 1 kHz is associated with the electron transfer at the Pt/electrolyte interface [30]. Under reverse bias, the TiO_2 is not significantly involved in the electron transfer, as the peak in the phase at 10 Hz is missing. The high resistance of the TCO/electrolyte interface determines the impedance signal. The attached dye at the TCO/electrolyte interface does not reduce the resistance as drastically as for set-up D, since

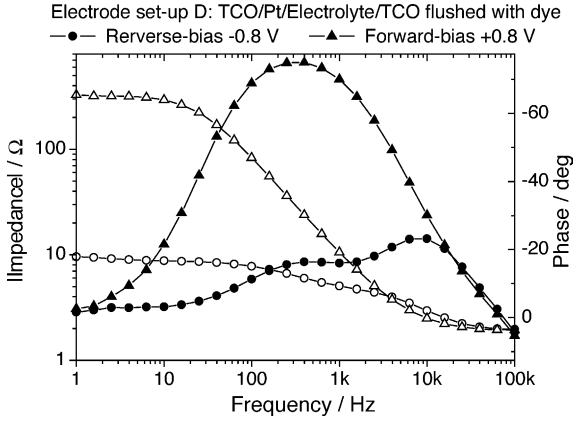

Fig. 9. Measured EIS of set-up D biased with +0.8 and −0.8 V. Open symbols: |*Z*|; solid symbols: phase (*Z*).

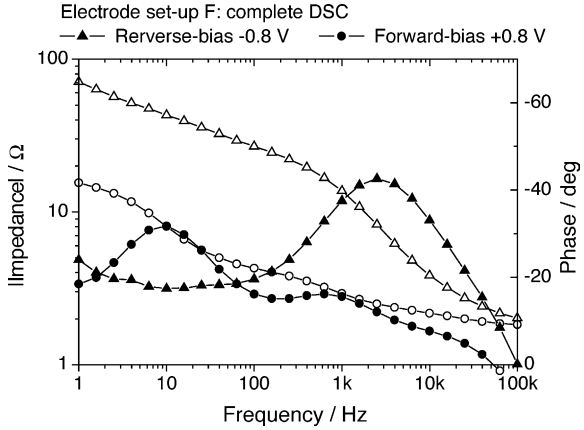

Fig. 10. Measured EIS of set-up F biased with +0.8 and −0.8 V. Open symbols: |*Z*|; solid symbols: phase (*Z*).

in this case the available surface of the TCO is much smaller due to the TiO_2.

4.4. Long term stability of reverse biased DSC

In terms of power output, the low breakdown voltage of a DSC is advantageous for the performance of DSC modules under partial shading. However, the long-term stability of a reverse biased DSC has to be addressed.

A shaded cell still has to transport the total current of the module. The voltage which is required to operate the shaded cell under this reverse current is determined by its *I–V* characteristic in reverse bias. A sufficiently large reverse biased voltage might therefore damage the cell, either by decomposition of the electrolyte solvent, or by damage to the dye. In practical terms, a potential greater than 1500 mV may damage a cell irreversibly [25].

The highest reverse current – and thus the highest reverse biased voltage – will occur when one cell is completely shaded and the module is operated under short-circuit conditions. Since all cells in a module should be electrically matched, the shaded cell then would conduct the equivalent of its own short-circuit current.

In order to simulate this worst-case situation, in Fig. 11 a DSC is shown, which is operated at a constant reverse current of 14 mA/cm^2 in the dark, corresponding to the cell's short-circuit current density under sun. The voltage drop over the cell was monitored for more than 100 h. This seems to be

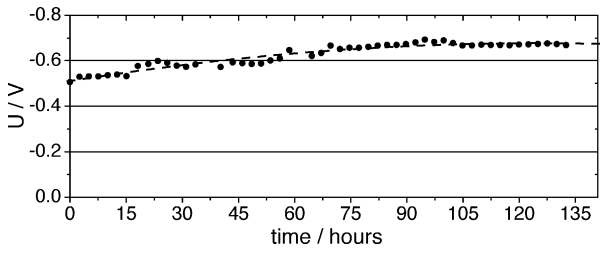

Fig. 11. A constant reverse current of 14 mA/cm^2 is applied to the cell. The voltage drop over the cell is monitored over time.

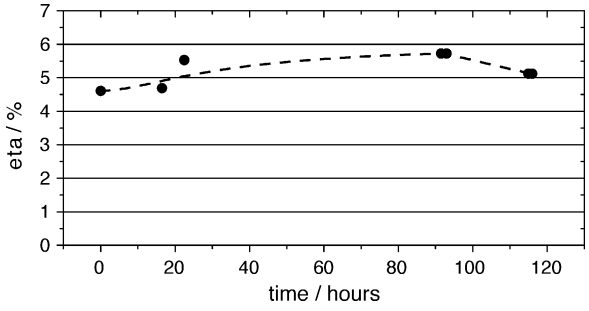

Fig. 12. A constant reverse current of 14 mA/cm^2 is applied to the cell. The efficiency of the cell is monitored over time.

a relevant time scale for the occasional partial shading of a module under outdoor conditions. For the first 60 h the voltage drop slowly rises at about 1.5 mV/h. It reaches saturation at a voltage below 0.7 V. The voltage seems to stay well below critical values of 1.5 V, which would damage the cell.

In Fig. 12, the efficiency of the cell was measured during the time of exposure to the reverse current. The efficiency is rising slightly and reaches saturation after about 20 h. The slight rise in efficiency was due to an increase of the fill factor.

In Fig. 13, the electrical impedance spectra of the cell are shown at different points in time during the exposure to the reverse current. The measurements were carried out in the dark at 720 mV forward bias, corresponding to the open-circuit voltage of the cell under sun. The amplitude of the modulated voltage was 5 mV.

The shift of the high frequency peak corresponds to a decrease in the charge transfer resistance at the Pt/electrolyte interface [30]. This conforms to the observed rise in fill factor.

It should be mentioned, that a blocking layer (apart from decreasing the power output of a partially shaded DSC module) might also reduce the stability of a partially shaded DSC module. The voltage required to run a DSC in reverse bias is significantly higher with an incorporated blocking layer [24]. However, no data to support this hypothesis is available yet.

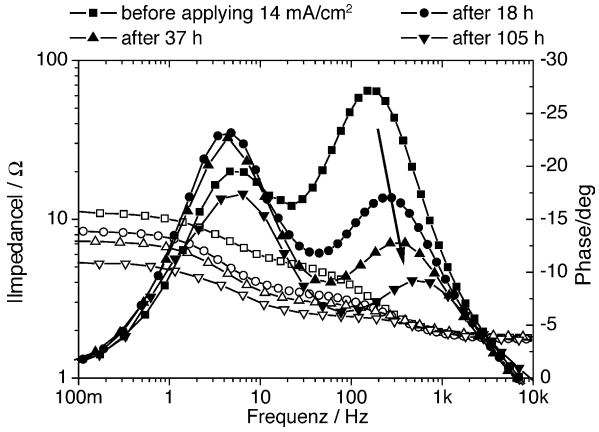

Fig. 13. A constant reverse current of 14 mA/cm^2 is applied to the cell. Electrical impedance spectra were measured at subsequent points in time. Open symbols: |*Z*|; solid symbols: phase (*Z*).

Furthermore, it should be noted that the stability of a DSC under reverse bias has only been demonstrated for a time scale, which seems relevant for the occasional partial shading of a module under outdoor conditions. In this work, all test cells showed an overall increase in conversion efficiency during the first 100 h of exposure to the reverse current. However, long term testing (>100 h) of reverse biased DSCs might still reveal degradation effects due to operation under reverse bias. The slight decrease in conversion efficiency between 90 and 110 h in Fig. 12 might indicate the beginning of such a long-term degradation. However, on a longer time scale more data must be collected to safely attribute this degradation to reverse biasing.

5. Conclusions

The processes and interfaces involved in the electron transport of a DSC under reverse bias were studied.

It was shown that charge transport under reverse bias directly occurs via the electrolyte/TCO interface, catalysed by the dye molecules. The charge transfer is highly asymmetrical, with a symmetry parameter of approximately 0.35, using a simple Butler-Vollmer model. Thus, the dye catalyses the electron transfer at the TCO/electrolyte interface only in reverse bias, but not under forward bias. Presumably, the dye undergoes a reversible oxidation, participating in the electron transfer reaction under reverse bias.

Electrical impedance spectroscopy revealed that in contrast to forward bias conditions, the TiO_2-layer is not significantly involved in the electron transport under reverse bias.

Due to the low breakdown voltage (approximately 500 mV under reverse bias), no bypass diodes are required when interconnecting DSC in modules, with respect to power output. With respect to long-term stability, no degradation in overall efficiency was observed after operating a DSC at a constant reverse current for 100 h. This seems a relevant time scale for the operation of a DSC module under outdoor conditions subjected to occasional partial shading. Degradation on a longer time scale (>100 h) due to operation under reverse bias must still be investigated. The magnitude of the reverse current applied to the DSC corresponded to the short circuit current of an illuminated cell in the module, in order to simulate the condition in a partially shaded DSC module.

It has to be noted though, that bypass diodes must be used over module terminals in case a cell or a group of cells undergoes degradation, for example, by leakage. Additionally, the reverse characteristic as well as the long-term stability under reverse bias for other types of electrolytes, e.g. pure ionic liquids, still has to be studied.

Acknowledgement

We would like to thank the Federal Ministry of Education and Research, Germany, for their financial support (FKZ 01SF0304).

References

[1] B. O'Regan, M. Gratzel, A low-cost, high-efficiency solar cell based on dye-sensitized colloidal TiO_2 films, Nature 353 (1991) 737–740.
[2] M. Gratzel, Perspectives for dye-sensitized nanocrystalline solar cells, Prog. Photovoltaics 8 (2000) 171–185.
[3] M.A. Green, K. Emery, K. Bucher, D.L. King, S. Igari, Solar cell efficiency tables (version 11), Prog. Photovoltaics 6 (1998) 35–42.
[4] H. Otaka, M. Kira, K. Yano, S. Ito, H. Mitekura, T. Kawata, F. Matsui, Multi-colored dye-sensitized solar cells, J. Photochem. Photobiol. A—Chem. 164 (2004) 67–73.
[5] G.E. Tulloch, Light and energy – dye solar cells for the 21st century, J. Photochem. Photobiol. A—Chem. 164 (2004) 209–219.
[6] M. Spath, P.M. Sommeling, J.A.M. van Roosmalen, H.J.P. Smit, N.P.G. van der Burg, D.R. Mahieu, N.J. Bakker, J.M. Kroon, Reproducible manufacturing of dye-sensitized solar cells on a semi-automated baseline, Prog. Photovoltaics 11 (2003) 207–220.
[7] A. Hinsch, J.M. Kroon, R. Kern, I. Uhlendorf, J. Holzbock, A. Meyer, J. Ferber, Long-term stability of dye-sensitised solar cells, Prog. Photovoltaics 9 (2001) 425–438.
[8] P. Wang, S.M. Zakeeruddin, J.E. Moser, M.K. Nazeeruddin, T. Sekiguchi, M. Gratzel, A stable quasi-solid-state dye-sensitized solar cell with an amphiphilic ruthenium sensitizer and polymer gel electrolyte, Nat. Mat. 2 (2003) 402–407.
[9] T. Toyoda, T. Sano, J. Nakajima, S. Doi, S. Fukumoto, A. Ito, T. Tohyama, M. Yoshida, T. Kanagawa, T. Motohiro, T. Shiga, K. Higuchi, K. Tanaka, Y. Takeda, T. Fukano, N. Katoh, A. Takeichi, K. Takechi, M. Shiozawa, Outdoor performance of large scale DSC modules, J. Photochem. Photobiol. A—Chem 164 (2004) 203–207.
[10] S. Dai, J. Weng, Y.F. Sui, C.W. Shi, Y. Huang, S.H. Chen, X. Pan, X.Q. Fang, L.H. Hu, F.T. Kong, K.J. Wang, Dye-sensitized solar cells, from cell to module, Sol. Energy Mater. Sol. Cells 84 (2004) 125–133.
[11] K. Okada, H. Matsui, T. Kawashima, T. Ezure, N. Tanabe, 100 mm × 100 mm large-sized dye sensitized solar cells, J. Photochem. Photobiol. A—Chem. 164 (2004) 193–198.
[12] S. Dai, K. Wang, J. Weng, Y. Sui, Y. Huang, S. Xiao, S. Chen, L. Hu, F. Kong, X. Pan et al., Design of DSC panel with efficiency more than 6%, Sol. Energy Mater. Sol. Cells 85, 447–455 (2005).
[13] A. Kovach, Effect of Partial Shading on the Ènergy Performance of Photovoltaic Arrays Integrated onto Buildings, VDI–Verlag GmBH, 1995.
[14] IEC_61215, Crystalline silicon terrestrial PV-modules—design qualification and type approval.
[15] IEC_61646, Thin-film terrestrial PV-modules—design qualification and type approval.
[16] S. Sodergren, A. Hagfeldt, J. Olsson, S.E. Lindquist, Theoretical-models for the action spectrum and the current–voltage characteristics of microporous semiconductor-films in photoelectrochemical cells, J. Phys. Chem. B 98 (1994) 5552–5556.
[17] F. Cao, G. Oskam, G.J. Meyer, P.C. Searson, Electron transport in porous nanocrystalline TiO_2 photoelectrochemical cells, J. Phys. Chem. B 100 (1996) 17021–17027.
[18] L. Dloczik, O. Ileperuma, I. Lauermann, L.M. Peter, E.A. Ponomarev, G. Redmond, N.J. Shaw, I. Uhlendorf, Dynamic response of dye-sensitized nanocrystalline solar cells: characterization by intensity-modulated photocurrent spectroscopy, J. Phys. Chem. B 101 (1997) 10281–10289.
[19] K. Schwarzburg, F. Willig, Origin of photovoltage and photocurrent in the nanoporous dye-sensitized electrochemical solar cell, J. Phys. Chem. B 103 (1999) 5743–5746.
[20] J. Ferber, R. Stangl, J. Luther, An electrical model of the dye-sensitized solar cell, Sol. Energy Mater. Sol. Cells 53 (1998) 29–54.

[21] J. Ferber, J. Luther, Modeling of photovoltage and photocurrent in dye-sensitized titanium dioxide solar cells, J. Phys. Chem. B 105 (2001) 4895–4903.
[22] R. Stangl, J. Ferber, J. Luther, On the modeling of the dye-sensitized solar cell, Sol. Energy Mater. Sol. Cells 54 (1998) 255–264.
[23] J.J. Lee, G.M. Coia, N.S. Lewis, Current density versus potential characteristics of dye-sensitized nanostructured semiconductor photoelectrodes. 1. Analytical expressions, J. Phys. Chem. B 108 (2004) 5269–5281.
[24] P. Cameron, L. Peter, S. Hore, How important is the back reaction of electrons via the substrate in dye-sensitized nanocrystalline solar cells? J. Phys. Chem. B 109 (2005) 930–936.
[25] M.G. Wheatley, A.M. McDonagh, M.P. Brungs, R.P. Chaplin, E. Sizgek, A study of reverse bias in a dye sensitised photoelectrochemical device, Sol. Energy Mater. Sol. Cells 76 (2003) 175–181.
[26] P.J. Cameron, L.M. Peter, Characterization of titanium dioxide blocking layers in dye-sensitized nanocrystalline solar cells, J. Phys. Chem. B 107 (2003) 14394–14400.
[27] P.J. Cameron, L.M. Peter, S.M. Zakeeruddin, M. Gratzel, Electrochemical studies of the Co(III)/Co(II)(dbbip)(2) redox couple as a mediator for dye-sensitized nanocrystalline solar cells, Coord. Chem. Rev. 248 (2004) 1447–1453.
[28] P.W. Atkins, Physikalische Chemie, VCH–Verlag, 1990.
[29] J. Nelson, Continuous-time random-walk model of electron transport in nanocrystalline TiO_2 electrodes, Phys. Rev. B 59 (1999) 15374–15380.
[30] R. Kern, R. Sastrawan, J. Ferber, R. Stangl, J. Luther, Modeling and interpretation of electrical impedance spectra of dye solar cells operated under open-circuit conditions, Electrochem. Acta 47 (2002) 4213–4225.